

# Journal of Materials Chemistry C

Accepted Manuscript



This is an *Accepted Manuscript*, which has been through the Royal Society of Chemistry peer review process and has been accepted for publication.

*Accepted Manuscripts* are published online shortly after acceptance, before technical editing, formatting and proof reading. Using this free service, authors can make their results available to the community, in citable form, before we publish the edited article. We will replace this *Accepted Manuscript* with the edited and formatted *Advance Article* as soon as it is available.

You can find more information about *Accepted Manuscripts* in the [Information for Authors](#).

Please note that technical editing may introduce minor changes to the text and/or graphics, which may alter content. The journal's standard [Terms & Conditions](#) and the [Ethical guidelines](#) still apply. In no event shall the Royal Society of Chemistry be held responsible for any errors or omissions in this *Accepted Manuscript* or any consequences arising from the use of any information it contains.

Cite this: DOI: 10.1039/c0xx00000x

www.rsc.org/xxxxxx

# Substituent effect on the electroluminescence efficiency of amidinate-ligated bis(pyridylphenyl) iridium(III) complexes

Virendra Kumar Rai,<sup>a</sup> Masayoshi Nishiura,<sup>a</sup> Masanori Takimoto<sup>a</sup> and Zhaomin Hou<sup>\*a</sup><sup>s</sup> Received (in XXX, XXX) Xth XXXXXXXXXX 20XX, Accepted Xth XXXXXXXXXX 20XX

DOI: 10.1039/b000000x

This paper reports the synthesis, structure, and photophysical and electrophosphorescence properties of heteroleptic amidinate/bis(pyridylphenyl) iridium(III) complexes having different substituents on the nitrogen atoms of the amidinate ancillary ligands. The reaction of bis(pyridylphenyl) iridium(III) chloride 10 [(ppy)<sub>2</sub>Ir(μ-Cl)]<sub>2</sub> with the lithium salt of various amidinate ligands Li{(NR)(NR')CPh} at 80 °C gave in 60–80% yields the corresponding heteroleptic bis(pyridylphenyl)/amidinate iridium(III) complexes having a general formula [(ppy)<sub>2</sub>Ir{(NR)(NR')CPh}], where R = R' = *i*-Pr (**1**), R = R' = *t*-Bu (**2**), R = Et, R' = *t*-Bu (**3**), and R = Et, R' = (CH<sub>2</sub>)<sub>3</sub>N(CH<sub>3</sub>)<sub>2</sub> (**4**). These heteroleptic iridium(III) complexes exhibited bright yellowish-green phosphorescence emission with moderate photoluminescence (PL) quantum yields (Φ<sub>PL</sub> 15 = 0.16–0.34) and short phosphorescence lifetimes of 0.98–1.18 μs in toluene solution at room temperature. Organic light-emitting diodes (OLEDs) were fabricated by the use of these complexes as phosphorescent dopants in various concentrations (*x* = 5–100 wt %) in the 4,4'-N,N'-dicarbazolylbiphenyl (CBP) host. Because of the steric hindrance of the amidinate ligands, no significant intermolecular interaction was observed in these complexes, thus leading to the reduction of self- 20 quenching and triple-triplet annihilation at high currents/luminance. Significant influence of the substituents in the amidinate ligands on the electroluminescence efficiency was observed. Among these complexes, complex (**2**), which contains the bulky *t*-butyl group on the amidinate nitrogen atoms, showed the highest current efficiency (η<sub>c</sub>: up to 116 cd A<sup>-1</sup>), power efficiency (η<sub>p</sub>: up to 72.2 lm W<sup>-1</sup>) and external quantum efficiency (η<sub>ext</sub>: up to 16.3 %).

25

## 1. Introduction

Organic light-emitting diodes (OLEDs) based on phosphorescent iridium(III) complexes are particularly promising because of their potential advantages of achieving a maximum internal efficiency 30 100%.<sup>1</sup> Therefore, many research groups have focused on the development of efficient OLEDs based on phosphorescent iridium(III) complexes.<sup>2–7</sup> In this context, heteroleptic cyclometalated (C<sup>^</sup>N) iridium(III) complexes [(C<sup>^</sup>N)<sub>2</sub>Ir(LX)], where LX = ancillary ligand] are very promising phosphorescent 35 materials due to easy synthetic chemical accessibility compared with the corresponding homoleptic Ir(C<sup>^</sup>N)<sub>3</sub> complexes.<sup>2c</sup> However, phosphorescent materials have some intrinsic disadvantages, such as saturation of emission sites due to an excessively long phosphorescent lifetime and concentration

40 quenching<sup>3</sup> arising from strong intermolecular interactions at high doping level,<sup>3a</sup> triplet-triplet (T-T) annihilation, and triplet-polaron (T-P) annihilation.<sup>2e,4</sup> To reduce self-quenching and annihilation, such phosphorescent materials always required doping into a charge-transporting host matrix. However, this 45 approach suffers from the poor reproducibility for mass production processes.<sup>5</sup> In addition, OLED based on these heteroleptic iridium(III) complexes exhibit significant efficiency roll-off at high current density and luminance due to strong (T-T) annihilation.<sup>6</sup> Since there are only a limited number of highly 50 efficient phosphorescent heteroleptic iridium(III) complexes for OLEDs, the current research interests in this area are mainly focused on exploiting new phosphorescent materials. The reduction in self-quenching and T-T annihilation can be realized

by introducing sterically demanding ancillary ligands into the phosphorescent emitters; however, its application to phosphorescent complexes remained almost unexploited. Therefore, it is highly desirable that the designed phosphorescent iridium(III) complexes can permit a complete energy transfer between the host and dopant in devices, while causing little or no self-quenching even at sufficiently high doping concentrations.

In our previous studies, we used the sterically demanding amidinate ancillary ligand [N,N'-diisopropylbenzamidinate;  $\{(N^iPr)_2CPh\}$ ] as a secondary ancillary ligand (LX) in the heteroleptic iridium complexes with various cyclometalated ligands  $[(C^AN)_2Ir\{(N^iPr)_2CPh\}]$  to develop highly efficient heteroleptic iridium(III) complexes for a wide range of emission colour.<sup>7</sup> The EL devices based on the amidinate-ligated complexes showed significant improvement in their emitting properties, such as reduction in self-quenching and insensitivity to doping-concentration. However, only isopropyl substituted amidinate ligand  $\{(N^iPr)_2CPh\}$  was employed and ligand effect of the amidinate ligand was not well investigated and optimized. Although there are two substituents on two nitrogen atoms and a substituent on the central carbon atom of an amidinate ligand, we became interested in the substituents on the nitrogen atoms because they are close to the central iridium atom and more significant substituent effect can be expected than that on the carbon.

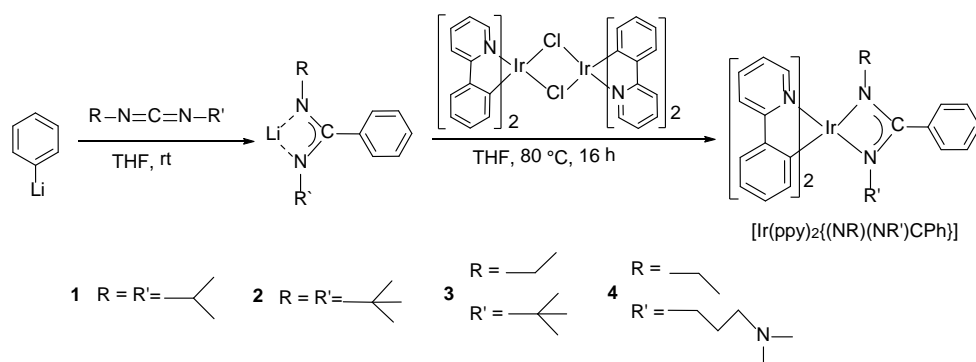
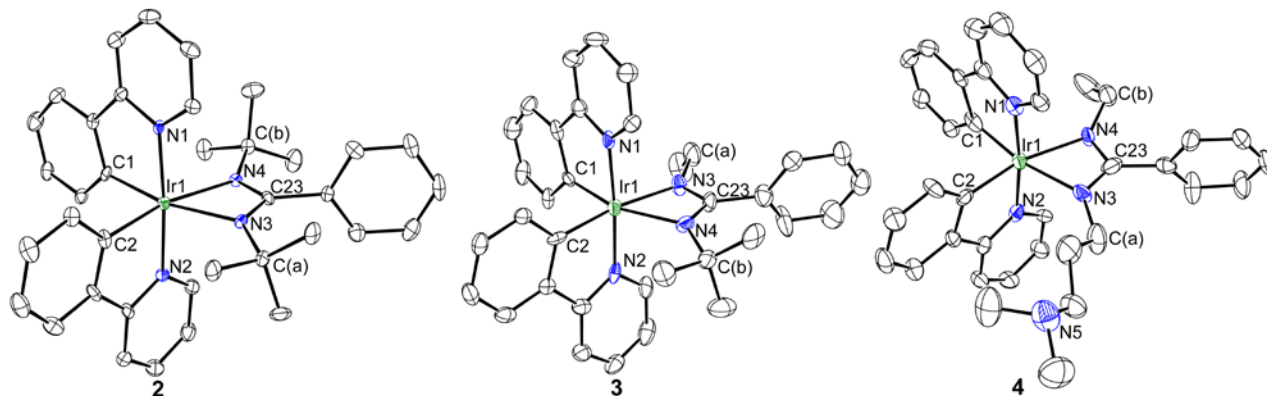
Herein, we report the synthesis, structural characterization, and photophysical, electrochemical and EL properties of a series of yellowish green heteroleptic bis-(pyridylphenyl)/amidinate iridium(III) complexes with various substituents on nitrogen atoms of amidinate ancillary ligands  $[(ppy)_2Ir\{(NR)(NR')CPh\}]$ , where R= R' = *i*Pr (**1**), R= R' = *t*-butyl (**2**), R= ethyl, R' = *t*-butyl (**3**), and R= ethyl, R' =  $(CH_2)_3N(CH_3)_2$  (**4**). Significant ligand effect was observed and the iridium complex with *t*-butyl substituted amidinate ligand (**2**) showed the highest EL device efficiency among these complexes.

## 2. Results and Discussion

### 2.1 Synthesis and Characterization of $[(ppy)_2Ir\{(NR)(NR')CPh\}]$ Complexes

The one-pot reaction of phenyl-lithium with carbodiimide, followed by refluxing with  $[(ppy)_2Ir(\mu-Cl)]_2$  in THF afforded the amidinate-ligated iridium(III) complexes  $[(ppy)_2Ir\{(NR)(NR')CPh\}]$  (**1-4**) in 60-80% yields (Scheme 1). These complexes are thermally stable and can be easily sublimed under vacuum. All of these complexes have been fully characterized by <sup>1</sup>H NMR, <sup>13</sup>C NMR, X-ray diffraction and micro-elemental analyses. The ppy ligands in **1**, **2**, and **4** showed one set of <sup>1</sup>H and <sup>13</sup>C NMR signals, but complex **3** showed two set of <sup>1</sup>H and <sup>13</sup>C NMR signals, because of the large difference between *t*-butyl and ethyl groups in the amidinate ligand. The methyl groups in complex **1** and the methylene group in **3**

showed two set of <sup>1</sup>H NMR signals, indicating that the rotation of the N-C bond in the amidinate ligands is highly restricted. Figure 1 shows the ORTEP diagrams of complexes (**2-4**). There are two independent molecules of **3** in the unit cell, and only one is shown. Selected bond lengths and angles are summarized in Table 1. The central iridium metal is coordinated by two bidentate phenylpyridine (ppy) and one monoanionic bidentate amidinate ligand to form distorted octahedral geometry. The coordination geometry of  $(ppy)_2$ -Ir fragments in the complexes **1-4** is similar to those reported for  $[(ppy)_2Ir(\mu-Cl)]_2$ <sup>8a</sup> and  $[(ppy)_2Ir(acac)]$ <sup>2c</sup>, in which the *cis*-C,C and *trans*-N,N coordination modes are observed. The average bond lengths of Ir-C (av. 1.984 (7) Å) and Ir-N(pyridyl) (av. 2.020(6) Å) in complexes **1-4** are comparable with those in  $[Ir(ppy)_2(acac)]$  [Ir-C, av. 2.003(9) Å; Ir-N, 2.010(9) Å], respectively.<sup>2c</sup> The bond lengths of the Ir-N(amidinate) bonds (av. 2.162(6) Å) in **1-4** are longer than those of the Ir-N(ppy) bonds (av. 2.020(6) Å). To see possible influences of the substituents at the N atom of amidinate ligand on the structure of the complexes, the dihedral angles of N(3,4)-C23-Ph(*ipso*)-Ph(*ortho*) were examined. It was found that the substituents at the N atom showed significant influence of these dihedral angles. The average value (89.0°) of the two smallest dihedral angles among N(3,4)-C23-Ph(*ipso*)-Ph(*ortho*) in complex **2**, which has bulky *t*-butyl substituents, is significantly larger than those of complexes **1** (70.3°), **3** (82.2°) and **4** (81.0°). The average bond angle (128.2°) of C23-N(3,4)-C(a,b) in **2** is larger than those of complexes **1** (125.4°), **3** (125.6°) and **4** (123.7°), probably because of the steric repulsion between the phenyl group and alkyl substituents on the nitrogen atoms. The crystal packing structures of complexes (**1-4**) (See SI Figure S1) revealed that the distances between two nearest parallel ppy planes were more than 3.6 Å, and no significant intermolecular  $\pi$ - $\pi$  interaction was observed.

**Scheme 1** Synthesis of  $[(ppy)_2Ir\{(NR)(NR')CPh\}]$  complexes.**Fig. 1** ORTEP diagrams of complexes **2**, **3**, and **4** with 30% thermal ellipsoids. Hydrogen atoms have been omitted for clarity.**Table 1** Selected bond lengths (Å) and bond angles (°) of complexes **1-4**.

(Å)	<b>1</b> <sup>7a</sup>	<b>2</b>	<b>3</b>	<b>4</b>
Ir(1)-C(1)	2.003(4)	2.013(6)	1.948(10)	1.929(12)
Ir(1)-C(2)	2.015(4)	2.018(6)	1.987(10)	1.962(10)
Ir(1)-N(1)	2.045(3)	2.047(4)	1.986(8)	2.020(9)
Ir(1)-N(2)	2.040(3)	2.050(5)	1.978(9)	1.996(9)
Ir(1)-N(3)	2.186(3)	2.180(5)	2.170(8)	2.136(9)
Ir(1)-N(4)	2.177(3)	2.177(5)	2.122(9)	2.152(8)
(°)				
C(1)-Ir(1)-N(3)	166.59(13)	166.3(2)	160.9(4)	168.2(4)
C(1)-Ir(1)-N(4)	106.93(14)	107.2(2)	100.4(4)	108.5(3)
C(2)-Ir(1)-C(1)	87.77(15)	85.6(2)	87.6(4)	85.9(4)
C(2)-Ir(1)-N(3)	105.28(15)	107.5(2)	111.2(3)	105.2(4)
N(2)-Ir(1)-N(1)	174.23(12)	175.23(19)	175.2(3)	173.3(4)
N(3)-Ir(1)-N(4)	60.36(13)	60.20(17)	61.1(3)	60.7(3)
C(23)-N(3)-C(a)	125.1(3)	128.2(5)	125.1(10)	122.6(10)
C(23)-N(4)-C(b)	125.7(4)	128.1(5)	126.0(9)	124.8(10)
Ir-N3N4-C23-Ph( <i>ipso</i> )planarity	0.02	0.02	0.03	0.03
N3-C23-Ph( <i>ipso</i> )-Ph( <i>ortho</i> )	70.0(7)	87.6(8)	86(2)	81(2)
N4-C23-Ph( <i>ipso</i> )-Ph( <i>ortho</i> )	70.7(6)	90.4(8)	78.5(2)	81(1)

**Table 2** Photophysical properties of complexes (1-4)

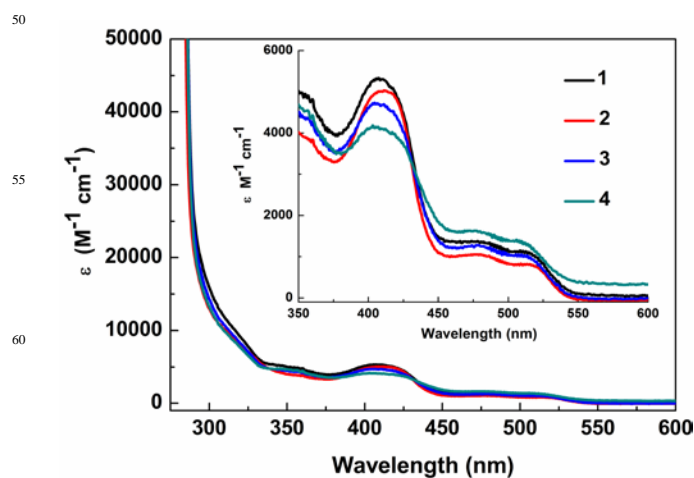
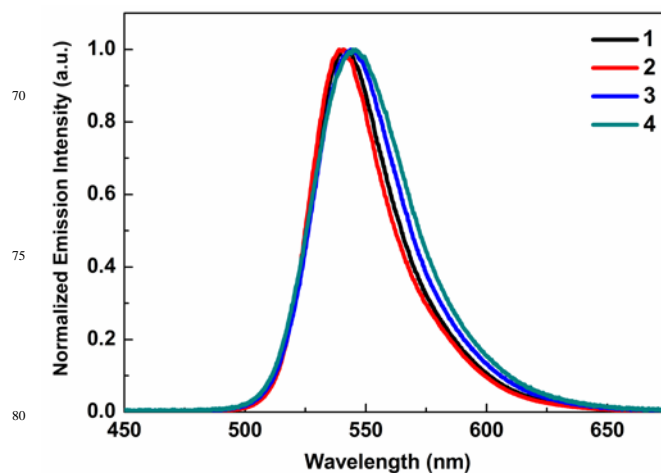
	Absorption $\lambda_{\max}$ ( $\epsilon \times 10^3 \text{ M}^{-1} \text{ cm}^{-1}$ )	Emission $\lambda_{\max}$ (nm)					
		solution	solid	$\tau$ ( $\mu\text{s}$ ) <sup>a</sup>	$\Phi_{\text{PL}}$ <sup>b</sup>	$k_r$ ( $10^5 \text{ s}^{-1}$ ) <sup>c</sup>	$k_{\text{nr}}$ ( $10^5 \text{ s}^{-1}$ ) <sup>d</sup>
1.	320 (9.10), 356 (4.85), 410 (5.30), 480 (1.34), 515 (1.11).	542	548	1.18	0.23	1.94	6.52
2.	320 (8.13), 358 (3.85), 412 (5.02), 480 (1.05), 515 (0.80).	542	546	1.14	0.34	2.98	5.78
3.	318 (8.76), 357 (4.35), 412 (4.64), 478 (1.28), 512 (1.02).	545	550	1.13	0.23	2.03	6.81
4.	315 (8.74), 357 (4.54), 410 (4.10), 478 (1.61), 508 (1.39).	546	552	0.98	0.16	1.63	8.57

<sup>a</sup> Phosphorescent life time were measured in toluene solution at room temp. <sup>b</sup> PL quantum yield in toluene solution. <sup>c</sup> Radiative decay rate  $k_r = \Phi/\tau$ . <sup>d</sup> Nonradiative decay rate  $k_{\text{nr}} = (1 - \Phi)/\tau$ . The experimental error range is  $\pm 1\%$  for lifetimes and  $\pm 5\%$  for quantum yields.

## 2.2 Photophysical Properties of [(ppy)<sub>2</sub>Ir{(NR)(NR')CPh}] Complexes

Absorption and emission spectra of complexes **1-4** in toluene solution are compiled in Fig. 2 and 3, respectively and the data are summarized in Table 2. Complexes **1-4** showed almost the similar absorption spectra in the range of 250-550 nm (Table 2 and Fig. 2). These complexes exhibited intense bands ( $\epsilon > 10^4 \text{ M}^{-1} \text{ cm}^{-1}$ ) at high energy (250–280 nm) and ( $\epsilon > 10^3 \text{ M}^{-1} \text{ cm}^{-1}$ ) at 320–358 nm, assignable to spin-allowed ligand-centered <sup>1</sup>LC ( $\pi$ - $\pi^*$ ) transitions of ppy ligands. The absorption bands observed at lower energies extending into the spectral region from 360–410 nm with extinction coefficient of  $\sim 5000$  to  $4000 \text{ M}^{-1} \text{ cm}^{-1}$  can also be assigned to spin-allowed (<sup>1</sup> $\pi$ - $\pi^*$ ) ppy and ancillary aromatic moieties along with minor contribution from metal-to-ligand charge transfer <sup>1</sup>MLCT transition. These MLCT bands are attributed to an effective mixing of charge-transfer transitions with higher lying spin-allowed transition on the ppy ligands. The lower-energy weak shoulder peaks extending into the region of 450 to 550 nm with extinction coefficient of  $\sim 2000$  to  $400 \text{ M}^{-1} \text{ cm}^{-1}$  are mainly derived from a spin-forbidden ligand-centered (<sup>3</sup> $\pi$ - $\pi^*$ ) transitions and as well as <sup>3</sup>MLCT contribution, due to the substantial reduction in the absorption extinction coefficient (Fig. 2 inset).

Complexes **1-4** in a degassed toluene solution at room temperature showed almost same PL spectra with intensive emissions at 542-546 nm under UV-light excitation at 350 nm (Fig. 3 and Table 2). The excited-states for emission of all complexes **1-4** have been identified as ligand centered transition [<sup>3</sup>LC( $\pi$ - $\pi^*$ )(ppy)] with significant MLCT [ $d\pi$ -(Ir)- $\pi^*$ (ppy)] character. The  $\lambda_{\max}$  of the PL spectrum of **1-4** showed ca. 4-6 nm red shift in solid state compared to that in solution (Table 2). The photoluminescence quantum yield ( $\Phi_{\text{PL}}$ ) increased in the order of  $2 > 1 = 3 > 4$  (Table 2), in agreement with the order of the steric hindrance of the amidinate ligands of these complexes. The  $\Phi_{\text{PL}}$  value (0.34) of **2** that bears two *t*-butyl groups on the nitrogen atoms of the amidinate ligand is higher than that ( $\Phi_{\text{PL}} = 0.25$ ) of the acac supported analogue [(ppy)<sub>2</sub>Ir(acac)],<sup>9a</sup> while the latter is comparable with that (0.23) of complexes **1** and **3**. The phosphorescent lifetimes of complexes **1-4** in toluene solution at room temperature are in the range of 0.98-1.18  $\mu\text{s}$  (Table 2; See SI Figure S2), which are shorter than that of the acac-coordinated complex [(ppy)<sub>2</sub>Ir(acac)] (1.6  $\mu\text{s}$ ).

**Fig. 2** UV-vis spectra of complexes **1-4** in toluene**Fig. 3** Photoluminescence spectra of complexes **1-4** in toluene

The relatively short phosphorescent lifetimes may allow the design and fabrication of highly efficient OLEDs because a short phosphorescent lifetime could decrease the detrimental T-T annihilation process. The radiative decay rates ( $k_r$ ) of the amidinate complexes **1-4** range from ( $1.6 \times 10^5 \text{ S}^{-1}$ ) to ( $2.9 \times 10^5 \text{ S}^{-1}$ ), and are similar to that of the acac analogue [(ppy)<sub>2</sub>Ir(acac)] ( $2.1 \times 10^5 \text{ S}^{-1}$ ).

### 2.3 Cyclic Voltammetry Studies

To ascertain the effects of individual substituents on the redox behavior of iridium(III)/ amidinate ligated complexes, cyclic voltammetry experiments were performed on all complexes (**1-4**). The cyclic voltammograms and summary of redox potentials are given in Figure S3 and Table 3, respectively. All four complexes exhibited reversible redox behavior at a scan-rate of 100 mVs<sup>-1</sup>. These complexes showed two oxidation peaks (ranging from +0.20 to +0.27 and from +0.74 to +1.12 V, respectively) and one reduction peaks (ranging from -2.47 to -2.73 V), in contrast with the acac analogue [(ppy)<sub>2</sub>Ir(acac)], which showed only one oxidation peaks (+0.42 V) and one reduction peaks (-2.52 V).<sup>9a,b</sup> This oxidation is analogous to remove an electron from the metal centered highest occupied molecular orbital (HOMO) level and the reduction is equivalent to the addition of an electron to the ppy-centered lowest unoccupied molecular orbital (LUMO) level.<sup>9</sup> Therefore, the first oxidation peaks of complexes **1-4** are attributable to oxidation from Ir-ppy moiety and the second oxidation peaks could result from oxidation of the amidinate unit {(NR)<sub>2</sub>CPh}.<sup>7</sup> The reduction peaks of **1-4** at negative potential ca. -2.47 to -2.73 V could be assigned to reduction of pyridyl ring of the ppy ligands as reported for other iridium(III) complexes bearing ppy ligand.<sup>9</sup>

On the basis of the first oxidation potential and optical absorption edge of the UV-vis spectra, the highest occupied molecular orbital (HOMO), the lowest unoccupied molecular orbital (LUMO), and the energy gap (E<sub>g</sub>) were calculated.<sup>10</sup> The HOMO energy levels (from -4.86 to -4.78 eV) of **1-4** are much higher than those of the iridium complexes such as [(ppy)<sub>2</sub>Ir(acac)] (-5.60 eV)<sup>1d</sup> and Ir(ppy)<sub>3</sub> (-5.40 eV)<sup>1b</sup>, which leads to a better hole-injection (HI) and hole-transport (HT) ability in OLEDs. The HOMO-LUMO energy gaps (E<sub>g</sub>) for the iridium(III) complexes (**1-4**) range from 2.25 to 2.27 eV. These values are consistent with the results of the maximum emission wavelength.

**Table 3.** Electrochemical data of [(ppy)<sub>2</sub>Ir{(NR)(NR')CPh}]\*

Ir(III) complex	E <sup>ox</sup> (V)	E <sup>red</sup> (V)	E <sub>g</sub> (eV)	HOMO (eV)	LUMO (eV)
<b>1</b>	+0.27, +0.74	-2.70	2.27	-4.85	-2.58
<b>2</b>	+0.26, +0.95	-2.73	2.26	-4.86	-2.60
<b>3</b>	+0.26, +1.12	-2.68	2.26	-4.84	-2.58
<b>4</b>	+0.20, +0.75	-2.47	2.25	-4.78	-2.53

\*0.1 M [TBAP] in CH<sub>3</sub>CN versus Ag/Ag + couple. HOMO = (E<sup>ox</sup> - E<sup>ox</sup><sub>(Fc/Fc<sup>+</sup>)</sub>) + (4.8 eV) and LUMO = HOMO + Bandgap (E<sub>g</sub>) was estimated from the onset wavelength of the optical absorption edge.

### 2.4 Electroluminescence (EL) Properties of [(ppy)<sub>2</sub>Ir{(NR)(NR')CPh}] Complexes

To evaluate the electroluminescence (EL) properties of the amidinate ligated iridium(III) complexes, organic light-emitting diodes (OLEDs) were fabricated by using complexes **1-4** as phosphorescent dopants at different doping concentrations (5, 10, 20, and 100 wt%) in 4,4'-N,N'-dicarbazolylbiphenyl (CBP) host molecule, respectively. Fig. 4 shows the materials structure, device configuration and energy level diagram of OLEDs devices used in this study. The devices consist of multilayer films with the same configuration of ITO/4,4'-bis(N-(1-naphthyl)-N-phenylamino)-biphenyl (NPB)(30 nm, hole-transporting layer)/CBP+[(ppy)<sub>2</sub>Ir{(NR)(NR')CPh}] (**1-4**) (x wt%) (35 nm, emitting layer)/2,9-dimethyl-4,7-diphenylphenanthroline (BCP) (6 nm, hole-blocking layer)/ tris(8-hydroxyquinoline) aluminium (Alq<sub>3</sub>) (25 nm, electron-transporting layer)/LiF (1 nm)/Al (100 nm). Fig. 5 shows the electroluminescence (EL) spectra of all complexes at 5 wt % doping concentration in CBP host. All devices exhibited bright yellowish-green emission around 550 nm with a broad wavelength range, which is suitable for white light emitting OLEDs to enhance colour rendering index (CRI).<sup>8b</sup> The electroluminescence spectra of all complexes exhibited no significant changes on various current and bias voltages i.e. EL spectra are independent of applied voltages in the range of 2.6 V to 16 V (See SI Figures S4, S6, S7 and S9), and are similar to those of the photoluminescence (PL) in solid-state, indicating no significant aggregation and self-quenching in these complexes. EL data of complexes (**1-4**) at different doping concentrations from 5 wt% to 100% (non-doped) are summarized in Table 4. All devices exhibited low turn-on voltages from 2.6 to 4.5 Volts. Moreover, the devices showed low driving voltages at the practical brightness of 100 cdm<sup>-2</sup> and 1000 cdm<sup>-2</sup> because of the narrow highest occupied molecular orbital (HOMO) and lowest unoccupied molecular orbital (LUMO) energy gap of complexes (**1-4**). As to the EL efficiency, significant influence of the substituents on the nitrogen atom of amidinate ancillary ligand was observed.

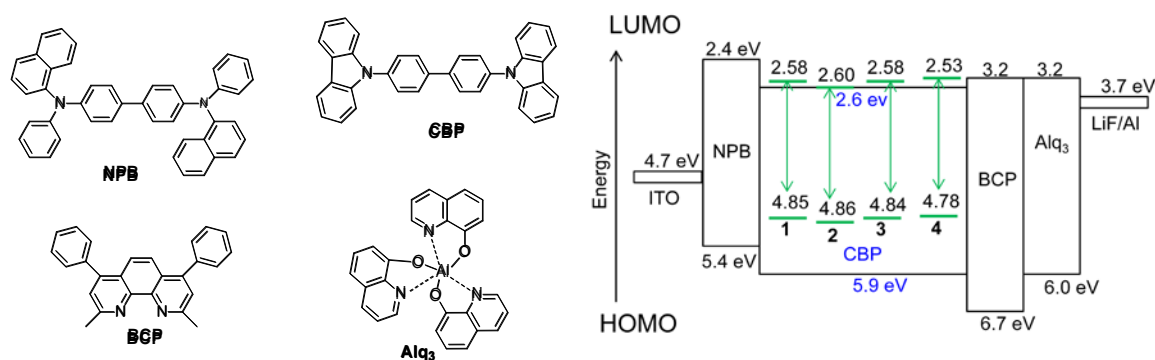


Fig. 4 Materials structure, device configuration with energy level diagram of OLEDs device.

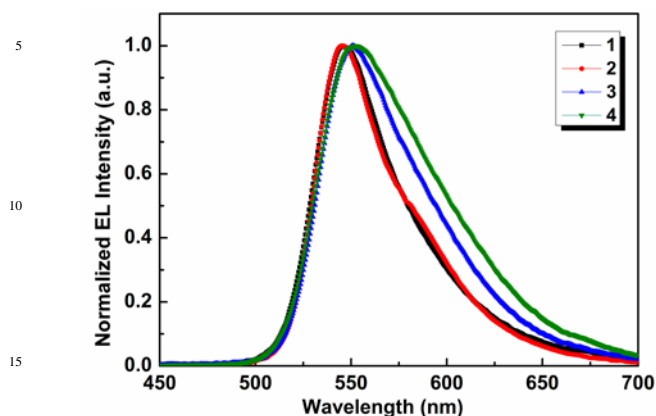
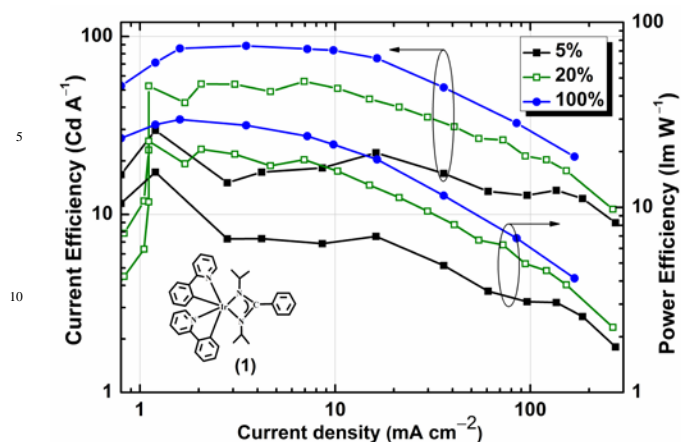


Fig. 5 EL spectra of complexes 1-4 at 5wt % doped devices.

Table 4. Electroluminescence performances of complexes (1-4)

Ir(III) Complexes	Doping concentration (x wt %)	Turn-on voltage (Volts)	$L_{\max}$ ( $\text{cd m}^{-2}$ ) <sup>a</sup>	$\eta_{\text{c max}}$ ( $\text{cd A}^{-1}$ ) <sup>b</sup>	$\eta_{\text{p max}}$ ( $\text{lm W}^{-1}$ ) <sup>c</sup>	$\eta_{\text{ext (max)}}$ [%] <sup>d</sup>	EL $\lambda_{\max}$ (nm)	CIE coordinates (X, Y) at 9V
1	5%	3.5	24360	29.6	15.5	4.1	545	0.42, 0.56
	20%	3.5	28480	52.7	22.8	7.6	548	0.42, 0.56
	100%	3.0	35551	85.6	29.8	12.5	548	0.42, 0.56
2	5%	3.0	51970	59.5	15.5	8.4	546	0.43, 0.55
	10%	3.0	79513	77.9	47.5	10.9	546	0.43, 0.55
	20%	2.6	185136	116.0	72.2	16.3	547	0.44, 0.55
	50%	3.3	54604	36.0	33.3	5.1	548	0.44, 0.55
	100%	3.0	34258	98.1	30.2	12.3	548	0.44, 0.55
3	5%	4.0	15181	60.7	17.0	8.5	551	0.46, 0.52
	10%	3.8	40308	50.8	12.2	6.8	552	0.46, 0.52
	20%	4.0	30781	60.0	15.5	8.0	552	0.46, 0.52
	100%	4.0	19654	8.0	2.3	1.1	555	0.48, 0.50
4	5%	4.5	5946	5.0	2.3	2.2	552	0.47, 0.51
	100%	4.5	4358	3.2	1.5	0.78	555	0.47, 0.51

<sup>a</sup>Maximum luminance. <sup>b</sup>Maximum current efficiency. <sup>c</sup>Maximum power efficiency. <sup>d</sup>Maximum External Quantum Efficiency.



**Fig. 6** Current efficiency ( $\eta_c$ ) and power efficiency ( $\eta_p$ ) as a function of current density ( $J$ ) for devices based on complex (1)

Fig. 6 shows the current efficiency versus power efficiency of OLEDs with various doping concentrations (5, 20, 100 wt%) based on complex (1). The maximum current efficiency ( $\eta_c = 29.6$  to  $85.6 \text{ cd A}^{-1}$ ) and maximum power efficiency ( $\eta_p = 15.5 \text{ lm W}^{-1}$  to  $29.8 \text{ lm W}^{-1}$ ) increase as doping concentrations increase from 5 wt% to 100% (non-doped), respectively (Table 4). The device (100%; non-doped) showed highest quantum efficiency of  $12.5\%$  at current density of  $3.5 \text{ mA cm}^{-2}$  (Table 4).

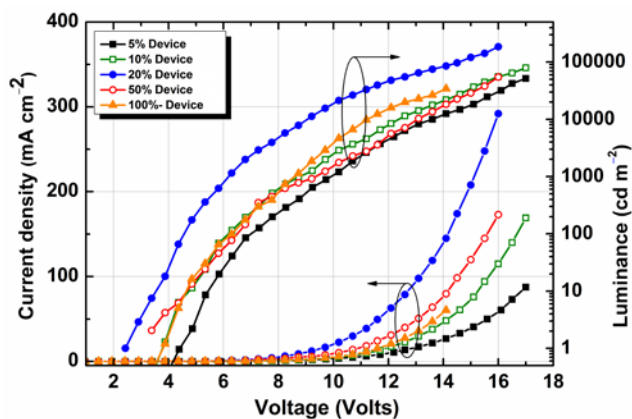


**Fig. 7** Current density ( $J$ ) and luminance ( $L$ ) characteristics as a function of voltage ( $V$ ) for devices based on complex (2).

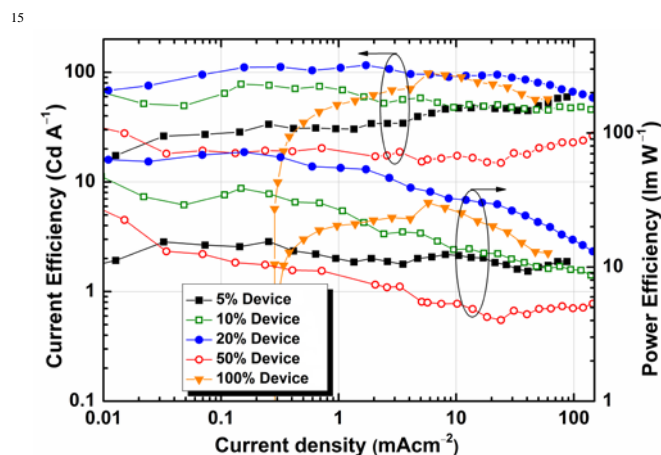


**Fig. 8** Current efficiency ( $\eta_c$ ) and power efficiency ( $\eta_p$ ) as a function of current density ( $J$ ) for devices based on complex (2)

Five different types of OLEDs devices at various doping concentrations (5, 10, 20, 50, 100 wt%) of complex 2 in CBP were fabricated. Fig. 7 shows current density-voltage-luminance ( $J$ - $V$ - $L$ ) characteristics of complex 2. The brightness gradually increased when the doping concentrations of complex 2 in CBP were increased up to 20% and finally decreased at higher doping concentrations from 50 wt% to 100% (non-doped) (Fig. 7, Table 4). The best device performance is achieved by device (20 wt%) with maximum luminance ( $L_{\text{max}}$ ) of  $185136 \text{ cd m}^{-2}$  at 16 V. This is the highest brightness of OLED reported in the literature from such a simple device configuration.<sup>1b,1d,2b,11</sup>

Fig. 8 shows current efficiency versus power efficiency of OLEDs based on complex 2. The current efficiency ( $\eta_c$ ) and power efficiency ( $\eta_p$ ) were increased with increasing doping concentration up to 20%, and reached to maximum current efficiency ( $\eta_c$ ) of  $111.0 \text{ cd A}^{-1}$  and power efficiency ( $\eta_p$ ) of  $72.2 \text{ lm W}^{-1}$ , respectively. This efficiency is the highest ever reported for an OLEDs at a similar doping level (*ca.* 20%).<sup>12</sup> More importantly, the power efficiency decayed gradually with increasing brightness, and the high power efficiency ( $31 \text{ lm W}^{-1}$ ) was observed even at high luminance of  $11280 \text{ cd m}^{-2}$  at current density of  $12.1 \text{ mA cm}^{-2}$ . The device (50 wt%) showed maximum current efficiency ( $\eta_c$ ) of  $36.0 \text{ cd A}^{-1}$  and maximum power efficiency ( $\eta_p$ ) of  $33.3 \text{ lm W}^{-1}$ . Finally, device (100%; non-doped) showed maximum current efficiency ( $\eta_c$ ) of  $98.1 \text{ cd A}^{-1}$  with maximum power efficiency ( $\eta_p$ ) of  $30.2 \text{ lm W}^{-1}$  and quantum efficiency of  $12.3\%$ . This device, as well as that based on 100% of 1, represents the most efficient non-doped phosphorescent OLED ever reported, as far as we are aware.<sup>13</sup>

Another feature that should be noted is that the quantum efficiency increases with increasing concentrations of complex 2 up to high doping levels (20 wt%), in contrast to [(ppy)<sub>2</sub>Ir(acac)] and Ir(ppy)<sub>3</sub> based devices, whose efficiency usually decreases at doping concentration higher than 10 wt%.

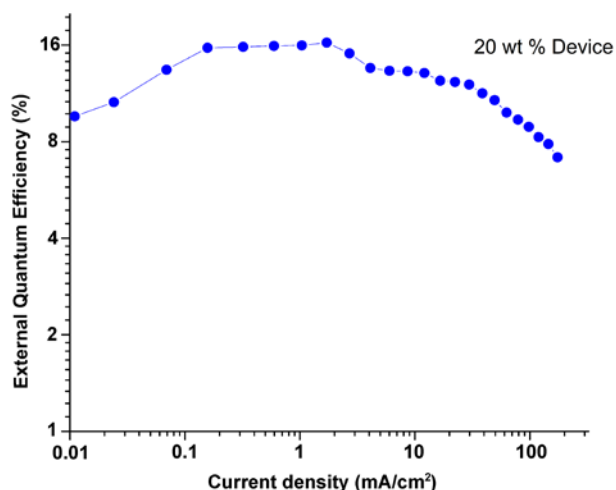


**Fig. 9** Current density ( $J$ ) versus quantum efficiency ( $\eta_{\text{ext}}$ ) characteristics of OLED at 20 wt % of complex (2) in CBP host

5

Fig. 9 shows the external quantum efficiency of OLED with 20wt% of complex 2 in CBP host as a function of current density. The external quantum efficiency reaches the maximum value 16.3% at  $1.71 \text{ mA cm}^{-2}$  and maintains relatively high values ( $>10\%$ ) even at high current densities (up to  $70 \text{ mA cm}^{-2}$ ). This is in contrast with a  $\text{Ir}(\text{ppy})_3$ -based device with 6% doping concentration in CBP host, whose external quantum efficiency reached the peak ( $\eta_{\text{ext}} = 14.6\%$ ) at a low current density (ca.  $0.01 \text{ mA cm}^{-2}$ ) and decreased with increasing current density.<sup>14a</sup>

15

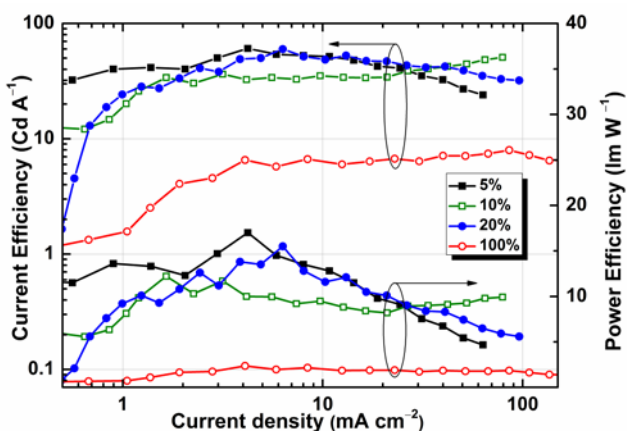


**Fig. 10** Current efficiency ( $\eta_c$ ) and power efficiency ( $\eta_p$ ) as a function of current density ( $J$ ) for devices based on complex (3)

20

Four different types of OLEDs devices at various doping concentrations (5, 10, 20, 100 wt%) of complex 3 in CBP were fabricated. Fig. 10 shows current efficiency versus power efficiency of OLEDs of complex 3 with ethyl and *t*-butyl groups on the nitrogen atoms of amidinate ligand. Devices (5, 10 and 20 wt%) showed maximum current efficiency ( $\eta_c = 60.7 \text{ cd A}^{-1}$ ,  $50.8$

25

$\text{cd A}^{-1}$  and  $60.0 \text{ cd A}^{-1}$ , respectively) and maximum power efficiency ( $\eta_p = 17.0 \text{ lm W}^{-1}$ ,  $12.2 \text{ lm W}^{-1}$  and  $15.5 \text{ lm W}^{-1}$ , respectively (Fig. 10, Table 4). It is noteworthy that the current efficiency and power efficiency of these devices relatively similar at a wide range of doping concentrations (5, 10 and 20 wt%). These results clearly demonstrate that the EL efficiency of complex 3 is not critically sensitive to doping concentrations. The non-doped device showed relatively lower efficiency (Fig. 10, Table 4). Complex (4) with ethyl and dimethylaminopropyl  $[(\text{CH}_2)_3\text{N}(\text{CH}_3)_2]$  groups on the nitrogen atoms of amidinate ligand showed poor efficiency (Table 4).

The EL efficiency of complexes 1-4 increases with increasing steric bulkiness of the alkyl substituents on the nitrogen atoms of the amidinate ligand, and complex 2 bearing two bulky *t*-butyl groups showed the highest EL efficiency. In the 20% doping concentration, the external quantum efficiency (16.3%) of 2 is almost as twice as those of 1 (7.6%) and 3 (8.0%) and this difference is larger than that of their PL quantum yields (1: 0.23, 2: 0.34, 3: 0.23). A possible reason of the high efficiency of 2 in PL and EL could be that significant effects on reduction of T-T or T-P annihilations and self-quenching/aggregation are induced by sterically-hindered *t*-butyl groups of the amidinate ancillary ligand to suppress intermolecular interaction. Another possible reason of high EL efficiency of 2 is that its LOMO level ( $-2.60 \text{ eV}$ ) is the same as that of the CBP host<sup>10d</sup> (Fig. 4), thus enabling efficient energy transfer from the host to the emitter 2 with reducing leakage of current in the devices.<sup>14</sup>

55

### 3. Conclusions

We have demonstrated that synthesis, structure, and photophysical and highly efficient electroluminescence properties of heteroleptic iridium(III) complexes  $[(\text{ppy})_2\text{Ir}\{(\text{NR})(\text{NR}')\text{CPh}\}]$  bearing various substituents on the nitrogen atoms of amidinate ancillary ligands. Significant influence of the substituents in the amidinate ancillary ligands on the electroluminescence efficiency has been observed and complex 2 with bulky *t*-butyl groups on both nitrogen atoms of amidinate ligand showed highest current efficiency ( $\eta_c$ ; up to  $116 \text{ cd A}^{-1}$ ), power efficiency ( $\eta_p$ ; up to  $72.2 \text{ lm W}^{-1}$ ) and external quantum efficiency ( $\eta_{\text{ext}}$ ; up to 16.3 %). These results clearly indicate that the incorporation of bulky groups on the nitrogen atoms of amidinate ligands is an effective way to avoid the self-quenching and reduction of T-T or T-A annihilations in phosphorescent devices at high luminance/currents.

70

## 4. Experimental Section

### 4.1 Materials and Methods

All reactions were carried out under a dry and oxygen-free nitrogen atmosphere by using Schlenk techniques or under a nitrogen atmosphere in an MBRAUN Lab master 130 glove box. The nitrogen was purified by being passed through a dry clean column (4A molecular sieves, Nikka Seiko Co.) and a Gas clean GC-XR column (Nikka Seiko Co.). The nitrogen in the glove box

80

was constantly circulated through a copper/molecular sieves catalyst unit. The oxygen and moisture concentrations in the glove box atmosphere were monitored by an O<sub>2</sub>/H<sub>2</sub>O Combi-Analyzer to ensure both were always below 0.1 ppm. Materials obtained from commercial supplier were used without further purification unless otherwise mentioned. THF, toluene and diethyl-ether (dehydrated, stabilizer-free) were obtained Kanto Kagaku Co. and purified by use of a MBRAUN SPS-800 solvent purification system. Samples for NMR spectroscopic measurements were prepared in the glove box by use of J. Young valve NMR tubes. NMR (<sup>1</sup>H, <sup>13</sup>C) spectra were recorded on a JNM-AL 300 spectrometer. Elemental analyses (C, H, N) were performed on a MICRO CORDER JM10 apparatus (J-SCIENCE LAB. Co.). The redox potential of iridium(III) complexes in acetonitrile was measured at scan rate 100 mV/s on a cyclic voltammeter (HSV-100-Hokuto Denko Corporation) with electrochemical work station, using a Pt working electrode, platinum wire as an auxiliary electrode, and Ag/AgNO<sub>3</sub> as a reference electrode under nitrogen atmosphere. Each measurement was calibrated with an internal standard, ferrocene/ferrocenium (Fc) redox system. The HOMO energy values were calculated based on the value of -4.8 eV for Fc with respect to zero vacuum level. Cyclometalated iridium(III) chloride [(ppy)<sub>2</sub>Ir(μ-Cl)]<sub>2</sub><sup>15</sup> and [(ppy)<sub>2</sub>Ir(N<sup>i</sup>Pr)<sub>2</sub>CPh] (**1**)<sup>7a</sup> were synthesized according to the literature procedure.

#### 4.2 Synthesis of [(ppy)<sub>2</sub>Ir{(NR)(NR')CPh}] Complexes

[(ppy)<sub>2</sub>Ir{(t-BuN)<sub>2</sub>CPh}] (**2**): In a 100 mL Schlenk flask, phenyllithium (0.21 mL, 0.4 mmol) was added to the solution of N,N'-di-*tert*-butyl-carbodiimide (62 mg, 0.4 mmol) in THF (5 mL) under argon at room temperature. The reaction mixture was stirred at room temperature for 2 h, and then reaction mixture was added dropwise to the chloride-bridge-iridium dimeric complex [(ppy)<sub>2</sub>Ir(μ-Cl)]<sub>2</sub> (220 mg, 0.2 mmol) in THF (15 mL). After being stirred at 80 °C for 16 h, the reaction mixture was cooled down to room temperature, and the solvent was evaporated under vacuum. In order to remove THF completely, the residue was dissolved in toluene and was evaporated under reduced pressure. The product was dissolved again in toluene and was filtered to remove lithium chloride. The crude product was washed with Et<sub>2</sub>O to give pure complex **2** (205 mg, 70% yield). Single crystals suitable for X-ray analysis were obtained by recrystallization in CH<sub>2</sub>Cl<sub>2</sub> solution. <sup>1</sup>H NMR (300 MHz, CDCl<sub>3</sub>, rt) δ 9.48 (d, *J* = 5.5 Hz, 2 H, aryl), 7.92 (d, *J* = 7.7 Hz, 2 H, aryl), 7.78 (t, *J* = 7.5 Hz, 2 H, aryl), 7.57 (d, *J* = 7.7 Hz, 2 H, aryl), 7.31-7.24 (m, 7 H, aryl), 6.76 (t, *J* = 7.1 Hz, 2 H, aryl), 6.62 (t, *J* = 7.3 Hz, 2 H, aryl), 6.22 (d, *J* = 7.3 Hz, 2 H, aryl), 0.44 (s, 18 H, *t*-butyl-CH<sub>3</sub>). <sup>13</sup>C NMR (75 MHz, CDCl<sub>3</sub>, rt) δ 169.5, 158.0, 150.9, 144.0, 143.3, 135.1, 131.6, 130.0, 128.9, 127.6, 127.0, 123.6, 121.0, 119.1, 118.0, 53.9, 33.7. Anal. Calcd. For C<sub>37</sub>H<sub>39</sub>IrN<sub>4</sub>: C, 60.71; H, 5.37; N, 7.65 Found: C, 60.88; H, 5.46; N, 7.78.

[(ppy)<sub>2</sub>Ir{(EtN)(*t*-BuN)CPh}] (**3**): According to the above-mentioned typical procedure, complex **3** (198 mg, 70% yield) was prepared from phenyllithium (0.21 mL, 0.4 mmol), 1-*tert*-

butyl-3-ethyl-carbodiimide (51 mg, 0.4 mmol) and [(ppy)<sub>2</sub>Ir(μ-Cl)]<sub>2</sub> (220 mg, 0.2 mmol) in THF (15 mL). Single crystals suitable for X-ray analysis were obtained by recrystallization in toluene solution. <sup>1</sup>H NMR (300 MHz, CDCl<sub>3</sub>, rt) δ 9.41 (d, *J* = 5.5 Hz, 1 H, aryl), 9.17 (d, *J* = 5.5 Hz, 1 H, aryl), 7.85-7.92 (m, 2 H, aryl), 7.77 (t, *J* = 9.7 Hz, 2 H, aryl), 7.60 (d, *J* = 7.3 Hz, 1 H, aryl), 7.55 (d, *J* = 7.7 Hz, 1 H, aryl), 7.16-7.36 (m, 10 H, aryl), 6.78 (m, 2 H, aryl), 6.67 (m, 2 H, aryl), 6.38 (d, *J* = 7.3 Hz, 1 H, aryl), 6.26 (d, *J* = 7.7 Hz, 1 H, aryl), 2.55-2.66 (m, 1 H, CH<sub>2</sub>-CH<sub>3</sub>), 2.30-2.41 (m, 1 H, CH<sub>2</sub>-CH<sub>3</sub>), 0.53 (s, 9 H, *t*-butyl-CH<sub>3</sub>), 0.18 (t, *J* = 7.1, 3 H, CH<sub>2</sub>-CH<sub>3</sub>). <sup>13</sup>C NMR (75 MHz, CDCl<sub>3</sub>, rt) δ 174.6, 169.7, 159.4, 155.0, 151.0, 150.2, 143.9, 143.8, 140.9, 135.5, 135.1, 132.4, 131.4, 129.0, 128.9, 128.7, 127.9, 127.6, 123.7, 123.4, 121.3, 121.1, 119.2, 119.1, 117.9, 117.7, 53.5, 40.7, 33.5, 16.9. Anal. Calcd for C<sub>35</sub>H<sub>35</sub>IrN<sub>4</sub>: C, 59.72; H, 5.01; N, 7.96 Found: C, 59.71; H, 5.24; N, 8.21.

[(ppy)<sub>2</sub>Ir{(EtN)(Me<sub>2</sub>N(CH<sub>2</sub>)<sub>3</sub>N)CPh}] (**4**): According to the above-mentioned typical procedure, complex **4** (205 mg, 70% yield) was prepared from phenyllithium (0.21 mL, 0.4 mmol), 1-ethyl-3-3-(dimethylaminopropyl) carbodiimide (62 mg, 0.4 mmol) and [(ppy)<sub>2</sub>Ir(μ-Cl)]<sub>2</sub> (220 mg, 0.2 mmol) in THF (15 mL). Single crystals suitable for X-ray analysis were obtained by recrystallization in CH<sub>2</sub>Cl<sub>2</sub>. <sup>1</sup>H NMR (300 MHz, CDCl<sub>3</sub>, rt) δ 9.10 (t, *J* = 5.3 Hz, 2 H, aryl), 7.88 (d, *J* = 8.0 Hz, 2 H, aryl), 7.74 (t, *J* = 7.5 Hz, 2 H, aryl), 7.58 (t, *J* = 6.6 Hz, 2 H, aryl), 7.40 (t, *J* = 7.9 Hz, 2 H, aryl), 7.16-7.21 (m, 5 H, aryl), 6.61-6.79 (m, 4 H, aryl), 6.37 (d, *J* = 6.6 Hz, 2 H, aryl), 2.82-2.90 (m, 2 H, (CH<sub>2</sub>)<sub>3</sub>N(CH<sub>3</sub>)<sub>2</sub>), 2.51-2.67 (m, 2 H, CH<sub>2</sub>-CH<sub>3</sub>), 1.75 (s, 6 H, N(CH<sub>3</sub>)<sub>2</sub>), 1.58-1.64 (m, 2 H, (CH<sub>2</sub>)<sub>3</sub>N(CH<sub>3</sub>)<sub>2</sub>), 0.86-0.94 (m, 2 H, (CH<sub>2</sub>)<sub>3</sub>N(CH<sub>3</sub>)<sub>2</sub>), 0.25 (t, *J* = 7.1 Hz, 3 H, CH<sub>2</sub>-CH<sub>3</sub>). <sup>13</sup>C NMR (75 MHz, CDCl<sub>3</sub>, rt) δ 176.0, 169.4, 156.5, 156.4, 150.5, 144.1, 136.3, 135.2, 132.2, 128.9, 128.8, 128.1, 123.6, 121.4, 119.4, 117.7, 57.29, 45.3, 44.9, 41.5, 30.0, 17.2. Anal. Calcd for C<sub>36</sub>H<sub>38</sub>IrN<sub>5</sub>: C, 58.99; H, 5.23; N, 9.56 Found: C, 59.19; H, 5.46; N, 9.58.

#### 4.3 Optical Measurements

The absorption and photoluminescence (PL) spectra of iridium(III) complexes in degassed dichloromethane have been measured on a Shimadzu UV-2550 UV-VIS spectrometer and on a fluorescence spectrometer Shimadzu RF-5301PC with a Xe arc lamp excitation source, respectively. The quantum yields were measured relative to quinine sulfate in 1N H<sub>2</sub>SO<sub>4</sub> assuming a quantum yield of 0.546 when excited at 350 nm. The solutions for the measurement were freshly prepared by dissolving the iridium complexes into spectroscopic grade CHCl<sub>3</sub>. Emission lifetime measurements were carried out by using a streak-camera based system (Hamamatsu, C4780) combined with a femto second Ti:sapphire laser system (Spectra-Physics, Spitfire). The excitation and detection wavelengths were 397 nm and 450–700 nm, respectively. The time resolution was 30–40 ns.

#### 4.4 OLED Fabrication and Characterization

Organic layers were fabricated by high-vacuum ( $10^{-4}$  Pa) thermal evaporation onto a glass substrate precoated with an indium-tin-oxide (ITO) layer (Sigma Aldrich) with a sheet resistance of 12-25  $\Omega/\square$ . Prior to use, the ITO (anode) surface was ultra sonicated in a detergent solution followed by a deionized water rinse, dipped into acetone, and 2-propanol, and then degreased in 2-propanol vapor. After degreasing, the substrate was kept in oven for dry at 80 °C for 2 hrs. Prior to organic film deposition, the ITO surface was treated with UV-Ozone chamber for 10 min before it was loaded into an evaporator. A 30 nm-thick layer of 4,4-bis(N-(1-naphthyl)-N-phenylamino)biphenyl (NPB) (Sigma Aldrich) act as a hole transport layer (HTL). The light emitting layer (35 nm) was consist of 5 to 50 wt % of iridium complexes doped into host 4,4'-N,N'-dicarbazolylbiphenyl (CBP) (Tokyo Chemical Industries, Co. Ltd.) as well as pure iridium complexes have been used. A 6 nm-thick 2,9-dimethyl-4,7-diphenyl-1,10-phenanthroline (BCP) (Tokyo Chemical Industries, Co. Ltd.) as a hole and exciton blocking layer (HBL) and tris(8-hydroxyquinoline)aluminum (Alq<sub>3</sub>) (Tokyo Chemical Industries, Co. Ltd.) (20 nm) as an electron transport layer (ETL) were deposited on the emitting layer. LiF layer (1 nm) was deposited at a rate of 1 Å/s serving as an electron injection layer (EIL). Finally Al (100 nm) electrode (cathode) was deposited at a rate of 10 Å/s. These all complexes have been vacuum deposited without any decomposition and shows very good film forming. The deposition rate for all organic layers was 1.0 Å/s. Thickness of the deposited layers was measured in-situ with a quartz crystal monitor. The size of each pixel was 5x5 mm<sup>2</sup>. The electroluminescence (EL) spectra have been measured on a high-resolution spectrometer (Stellar net Blue-wave UV-VIS-NIR). The current-voltage-luminescence (I-V-L) characteristics have been measured with a luminance meter (Chroma-Meter CS-200 Konika Minolta, Japan) and Keithley-2400 programmable voltage-current digital source meter. All the measurements were carried out at room temperature under ambient conditions.

#### 4.5 X-ray Crystallographic Studies

A crystal was sealed in a thin-walled glass capillary under a microscope. Data collections were performed at -100 °C on a Bruker SMART APEX diffractometer with a CCD area detector using graphite-monochromated MoK $\alpha$  radiation ( $\lambda = 0.71069$  Å). The determination of crystal class and unit cell parameters was carried out by the SMART program package.<sup>16</sup> The raw frame data were processed using SAINT<sup>17</sup> and SADABS<sup>18</sup> to yield the reflection data file. The structures were solved by using SHELXTL program.<sup>19</sup> Refinements were performed on  $F^2$  anisotropically for all the non-hydrogen atoms by the full-matrix least-squares method. The analytical scattering factors for neutral atoms were used throughout the analysis. The hydrogen atoms were placed at the calculated position and were included in the structure calculation without further refinement of the parameter. In the case of **3**, there are two independent molecules of the iridium complexes and one molecule of the toluene solvent in the unit cell, and two C-C bonds of the toluene molecule were fixed

to 1.41 Å. The disordered methyl groups in ethyl ligands in **3** were separated into two parts (C35, C71 and C70, C72) and were treated with 50% occupancy, respectively. The phenyl carbons (C59-C64) and the carbon (C65-C70, C72) atoms of ethyl and t-butyl groups in **3** were refined with the same anisotropic displacement parameters, respectively. The residual electron densities were of no chemical significance. Crystal data and processing parameters are summarized in Table (See SI Table S1). CCDC-908623 (**2**), 908624 (**3**), 908625 (**4**) contain the supplementary crystallographic data for this paper. These data can be obtained free of charge from The Cambridge Crystallographic Data Centre via [www.ccdc.cam.ac.uk/data\\_request/cif](http://www.ccdc.cam.ac.uk/data_request/cif).

#### Acknowledgements

This work was supported by a Grant-in-Aid for Scientific Research (S) (No. 21225004) (to Z.H.) and for Scientific Research (B) (No. 24350030) (to M.N.) from Japan Society for the Promotion of Science. The authors would like to thank to Prof. T. Tahara and Dr. K. Ishii for phosphorescence lifetime measurements, and Ms. A. Karube for elemental analysis.

#### Notes and references

<sup>a</sup>Organometallic Chemistry Laboratory, RIKEN, 2-1 Hirosawa, Wako, Saitama-351-0198, Japan; \*E-mail: [houz@riken.jp](mailto:houz@riken.jp)

† Electronic Supplementary Information (ESI) available: Crystallographic data in CIF format of complexes (**2-4**), phosphorescent lifetime, cyclic voltammograms, and performance data of all OLEDs. See DOI: 10.1039/b000000x/

- (a) M. A. Baldo, D. F. O'Brien, Y. You, A. Shoustikov, S. Sibley, M. E. Thompson and S. R. Forrest, *Nature*, 1998, **395**, 151; (b) M. A. Baldo, S. Lamansky, P. E. Burrows, M. E. Thompson and S. R. Forrest, *Appl. Phys. Lett.*, 1999, **75**, 4; (c) M. A. Baldo, M. E. Thompson and S. R. Forrest, *Nature*, 2000, **403**, 750; (d) C. Adachi, M. A. Baldo, M. E. Thompson and S. R. Forrest, *J. Appl. Phys.*, 2001, **90**, 5048; (e) Y. Sun, C. G. Noel, K. Hiroshi, M. Biwu, M. E. Thompson and S. R. Forrest, *Nature*, 2006, **440**, 908.
- (a) C. Adachi, M. A. Baldo and S. R. Forrest, *J. Appl. Phys.*, 2000, **87**, 8049; (b) M. Ikai, S. Tokito, Y. Sakamoto, T. Suzuki and Y. Taga, *Appl. Phys. Lett.*, 2001, **79**, 156; (c) S. Lamansky, P. Djurovich, D. Murphy, F. Abdel-Razzaq, R. Kwong, I. Tsyba, M. Bortz, B. Mui, R. Bau and M. E. Thompson, *Inorg. Chem.*, 2001, **40**, 1704; (d) S. Lamansky, P. Djurovich, D. Murphy, F. Abdel-Razzaq, H.-E. Lee, C. Adachi, P. E. Burrows, S. R. Forrest and M. E. Thompson, *J. Am. Chem. Soc.*, 2001, **123**, 4304; (e) C. Adachi, R. Kwong and S. R. Forrest, *Org. Electron.*, 2001, **2**, 37; (f) A. B. Tamayo, B. D. Alleyne, P. I. Djurovich, S. Lamansky, I. Tsyba, N. N. Ho, R. Bau, and M. E. Thompson, *J. Am. Chem. Soc.*, 2003, **125**, 7377; (g) U. Christoph, B. Beatrice, F. Christian, W. Andreas and S. S. Ulrich, *Adv. Mater.* 2009, **21**, 4418; (h) X. Lixin, C. Zhijian, Q. Bo, L. Jiaxiu, K. Sheng, G. Qihuang and K. Junji, *Adv. Mater.*, 2011, **23**, 926; (i) H.-H. Chou and C.-H. Cheng, *Adv. Mater.*, 2010, **22**, 2468; (j) Y. Chi and P.-T. Chou, *Chem. Soc. Rev.*, 2010, **39**, 638; (k) Y. Youngmin and Y. P. Soo, *Dalton Trans.*, 2009, 1267; (l) W.-Y. Wong and C.-L. Ho, *J. Mater. Chem.*, 2009, **19**, 4457; (m) Z. Q. Chen, Z. Q. Bian and C. H. Huang, *Adv. Mater.*, 2010, **22**, 1534; (n) J. A. G. Williams, A. J. Wilkinson and V. L. Whittle, *Dalton Trans.*, 2008, 2081.
- (a) M. A. Baldo, D. F. O'Brien, M. E. Thompson and S. R. Forrest, *Phys. Rev. B*, 1999, **60**, 14422; (b) Y. Kawamura, K. Goushi, J. Brooks, J. J. Brown, H. Sasabe and C. Adachi, *Appl. Phys. Lett.*, 2005, **86**, 071104; (c) E. B. Namdas, A. Ruseckas, I. D. W. Samuel, S.-C. Lo and P. L. Burn, *J. Phys. Chem. B*, 2004, **108**,

- 1570; (d) Y. Q. Zhang, G. Y. Zhong and X. A. Cao, *J. Appl. Phys.*, 2010, **108**, 083107.
- (4) (a) C. Adachi, M. A. Baldo, S. R. Forrest and M. E. Thompson, *Appl. Phys. Lett.*, 2000, **77**, 904; (b) W. Staroske, M. Pfeiffer, K. Leo and M. Hoffmann, *Phys. Rev. Lett.*, 2007, **98**, 197402; (c) S. Reineke, T. C. Rosenow, B. Lussem and K. Leo, *Adv. Mater.*, 2010, **22**, 3189; (d) S. Reineke, G. Schwartz, K. Walzer, M. Falke and K. Leo, *Appl. Phys. Lett.*, 2009, **94**, 163305; (e) W. S. Jeon, T. J. Park, S.-Y. Kim, R. Pode, J. Jang and J. H. Kwon, *Appl. Phys. Lett.*, 2008, **93**, 063303; (f) M.-Y. Teng, S. Zhang, S.-W. Jiang, X. Yang, C. Lin, Y.-X. Zheng, L. Wang, D. Wu, J.-L. Zuo and X.-Z. You, *Appl. Phys. Lett.*, 2012, **100**, 073303; (g) H.-Y. Lee, L. Zhou, M. Y. Teng, Q.-L. Xu, C. Lin, Y.-X. Zheng, J.-L. Zuo, H.-J. Zhang and X.-Z. You, *J. Mater. Chem. C*, 2013, **1**, 560.
- (5) (a) S. L. Lin, L. H. Chan, R. H. Lee, M. Y. Yen, W. J. Kuo, C. T. Chen and R. J. Jeng, *Adv. Mater.*, 2008, **20**, 3947; (b) Q. X. Tong, S. L. Lai, M. Y. Chan, Y. C. Zhou, H. L. Kwong, C. S. Lee and S. T. Lee, *Chem. Mater.*, 2008, **20**, 6310; (c) N. Li, S. L. Lai, P. F. Wang, F. Teng, Z. T. Liu, C. S. Lee and S. T. Lee, *Appl. Phys. Lett.*, 2009, **95**, 133301.
- (6) (a) M. A. Baldo, C. Adachi and S. R. Forrest, *Phys. Rev. B*, 2000, **62**, 10967; (b) Z. W. Liu, M. Guan, Z. Q. Bian, D. B. Nie, Z. L. Gong, Z. B. Li and C. H. Huang, *Adv. Funct. Mater.*, 2006, **16**, 1441; (c) J. W. Kang, S. H. Lee, H. D. Park, W. I. Jeong, K. M. Yoo, Y. S. Park and J. J. Kim, *Appl. Phys. Lett.*, 2007, **90**, 223508.
- (7) (a) Y. Liu, K. Ye, Y. Fan, W. Song, Y. Wang and Z. Hou, *Chem. Commun.*, 2009, 3699; (b) T. Peng, H. Bi, Y. Liu, Y. Fan, H. Gao, Y. Wang and Z. Hou, *J. Mater. Chem.*, 2009, **19**, 8072; (c) T. Peng, Y. Yang, Y. Liu, D. Ma, Z. Hou and Y. Wang, *Chem. Commun.*, 2011, **47**, 3150; (d) T. Peng, Y. Yang, H. Bi, Y. Liu, D. Ma, Z. Hou and Y. Wang, *J. Mater. Chem.*, 2011, **21**, 3551.
- (8) (a) F. O. Graces, K. Dedeian, N. L. Keder and R. J. Watts, *Acta Crystallogr.*, 1993, **C49**, 1117; (b) S. Reinkene, M. Thomschke, B. Lussem and K. Leo, *Rev. Mod. Phys.*, 2013, **85**, 1245.
- (9) (a) X. Li, Z. Chen, Q. Zhao, L. Shen, F. Li, T. Yi, Y. Cao and C. Huang, *Inorg. Chem.*, 2007, **46**, 5518; (b) M. Velusamy, K. R. J. Thomas, C.-H. Chen, J. T. Lin, Y. S. Wen, W.-T. Hsieh, C.-H. Lai and P.-T. Chou, *Dalton Trans.*, 2007, 3025; (c) M. S. Lowry, J. I. Goldsmith, J. D. Slinker, R. Richard, R. A. Pascal, G. G. Malliaras and S. Bernhard, *Chem. Mater.*, 2005, **17**, 5712; (d) J. Li, P. I. Djurovich, B. D. Alleyne, M. Yousufuddin, N. N. Ho, J. C. Thomas, J. C. Peters, R. Bau and M. E. Thompson, *Inorg. Chem.*, 2005, **44**, 1713; (e) C.-H. Yang, S.-W. Li, Y. Chi, Y.-M. Cheng, Y.-S. Yeh, P.-T. Chou, G.-H. Lee, C.-H. Wang and C.-F. Shu, *Inorg. Chem.*, 2005, **44**, 7770; (f) Y. Ohsawa, S. Sprouse, K. A. King, M. K. DeArmond, K. W. Hanck and R. J. Watts, *J. Phys. Chem.*, 1987, **91**, 1047; (g) J. Brooks, Y. Babayan, S. Lamansky, P. I. Djurovich, I. Tsyba, R. Bau and M. E. Thompson, *Inorg. Chem.*, 2002, **41**, 3055; (h) P. J. Hay, *J. Phys. Chem. A*, 2002, **106**, 1634.
- (10) (a) Y. C. Chia, H. C. Lu, C. G. Wu, J. G. Chen and K. C. Ho, *Adv. Funct. Mater.*, 2007, **17**, 29; (b) J. Pommerehne, H. Vestweber, W. Guss, R. F. Mahrt, H. Bassler, M. Porsch and J. Daub, *Adv. Mater.*, 1995, **7**, 551; (c) Y. Liu, H. Ma and A. K.-Y. Jen, *Chem. Mater.*, 1999, **11**, 27; (d) S. H. Kim, J. Jang and Y. Lee, *Appl. Phys. Lett.*, 2007, **91**, 083511.
- (11) (a) C. E. Nicholas and R. J. Holmes, *Appl. Phys. Lett.*, 2010, **97**, 083308; (b) L. Shumei, L. Bin, Z. Liming, S. Hang and J. Hong, *Appl. Phys. Lett.*, 2010, **97**, 083304; (c) Z. B. Wang, M. G. Helander, J. Qiu, D. P. Puzzo, M. T. Greiner, Z. W. Liu and Z. H. Lu, *Appl. Phys. Lett.*, 2011, **98**, 073310; (d) H. Gufeng, M. Pfeiffer, L. Karl, M. Hofmann, J. Birnstock, P. Robert and S. Josef, *Appl. Phys. Lett.*, 2004, **85**, 3911.
- (12) (a) Y. Wang, N. Herron, V. V. Grushin, D. LeCloux and V. Petrov, *Appl. Phys. Lett.*, 2001, **79**, 449; (b) H. Z. Xie, M. W. Liu, O. Y. Wang, X. H. Zhang, C. S. Lee, L. S. Hung, S. T. Lee, P. F. Teng, H. L. Kwong, Z. Hui and C. M. Che, *Adv. Mater.*, 2001, **13**, 1245; (c) R. J. Holmes, B. W. D'Andrade, S. R. Forrest, X. Ren, J. Li and M. E. Thompson, *Appl. Phys. Lett.*, 2003, **83**, 3818; (d) Y. H. Song, S. J. Yeh, C. T. Chen, Y. Chi, C. S. Liu, J. K. Yu, Y. H. Hu, P. T. Chou, S. M. Peng and G. H. Lee, *Adv. Funct. Mater.*, 2004, **14**, 1221. (e) Z. W. Liu, M. Guan, Z. Q. Bian, D. B. Nie, Z. L. Gong, Z. B. Li and C. H. Huang, *Adv. Funct. Mater.* 2006, **16**, 1441; (f) B. Liang, L. Wang, Y. H. Xu, H. H. Shi and Y. Cao, *Adv. Funct. Mater.*, 2007, **17**, 3580; (g) M. S. Park, H. J. Park, O. Y. Kim and Y. Lee, *Org. Electron.*, 2013, **14**, 1504.
- (13) (a) L. Chen, Z. Ma, J. Ding, L. Wang, X. Jing and F. Wang, *Chem. Commun.*, 2011, **47**, 9519; (b) S. Liu, B. Li, L. Zhang and S. Yue, *Appl. Phys. Lett.*, 2011, **98**, 163301; (c) S. Liu, B. Li, L. Zhang, H. Song and H. Jiang, *Appl. Phys. Lett.*, 2010, **98**, 083304; (d) J. Ding, B. Wang, Z. Yue, B. Yao, Z. Xie, Y. Cheng, L. Wang, X. Jing and F. Wang, *Angew. Chem. Int. Ed.*, 2009, **48**, 6664; (e) Z. Liu, Z. Bian, L. Ming, F. Ding, H. Shen, D. Nie and C. Huang, *Org. Electron.*, 2008, **9**, 171; (f) Y. H. Song, S. J. Yeh, C. T. Chen, Y. Chi, C. S. Liu, J. K. Yu, Y. H. Hu, P. T. Chou, S. M. Peng and G. H. Lee, *Adv. Funct. Mater.*, 2004, **14**, 1221; (g) H. Z. Xie, M. W. Liu, O. Y. Wang, X. H. Zhang, C. S. Lee, L. S. Hung, S. T. Lee, P. F. Teng, H. L. Kwong, Z. Hui and C. M. Che, *Adv. Mater.*, 2001, **13**, 1245.
- (14) (a) D. M. Kang, J.-W. Kang, J. W. Park, S. O. Jung, S.-H. Lee, H.-D. Park, Y.-H. Kim, S. C. Shin, J.-J. Kim and S.-K. Kwon, *Adv. Mater.*, 2008, **20**, 2003; (b) X. H. Yang, F. Jaiser, B. Stiller, D. Neher, F. Galbrecht and U. Scherf, *Adv. Funct. Mater.*, 2006, **16**, 2156; (c) X. H. Yang, D. C. Möller, D. Neher and K. Meerholz, *Adv. Mater.*, 2006, **18**, 948; (d) T. Suzuki and S. Tokito, *Adv. Mater.*, 2007, **19**, 276.
- (15) M. Nonoyama, *Bull. Chem. Soc. Jpn.* 1974, **47**, 767.
- (16) SMART Software, version 4.21; Bruker AXS, Inc., Madison, WI, 1997.
- (17) SAINT PLUS, version 6.02; Bruker AXS, Inc., Madison, WI, 1999.
- (18) G. M. Sheldrick, *SADABS*; Bruker AXS, Inc., Madison, WI, 1998.
- (19) G. M. Sheldrick, *SHELXTL*, version 5.1; Bruker AXS, Inc., Madison, WI, 1998.

**Table of Contents (TOC).**

Significant substituent effect on the EL properties was observed and heteroleptic iridium(III) complex with *t*-Bu substituted amidinate ligand  $[(ppy)_2Ir\{(t-BuN)_2CPh\}]$  showed high current and power efficiency.

